ACS OMEGA

http://pubs.acs.org/journal/acsodf

Article

Democratizing the Assessment of Thermal Robustness of Metal−Organic Frameworks

Satyanarayana Bonakala, Anas Abutaha, Palani Elumalai, Ayman Samara, Said Mansour, and Fedwa El-Mellouhi*

Cite This: *ACS Omega* 2022, 7, 46515−46523

Read Online

ACCESS | Metrics & More | Article Recommendations | Supporting Information

ABSTRACT: With the pressing need of having reliable materials for carbon dioxide capture, metal−organic frameworks (MOFs) have shown promising performance due to their flexible sign and tunable functionality by applying reticular chemistry principles. One of the main characteristics of practical MOFs is to design thermally robust candidates for sustainable functionality. Here, we introduce a comprehensive methodology for examining the thermal stability of MOFs by combining theoretical calculations and affordable experimental methods to fully describe their performance under thermal variations. We chose the prototypical MOF, HKUST-1, to assess the methodology by performing density functional theory and classical molecular dynamics simulations and validating with experiments such as in situ powder X-ray diffraction, differential scanning calorimetry, and thermogravimetric analysis. HKUST-1 shows thermal robustness until a temperature of 240 °C at different atmospheric gases with a reversible breathing trend with temperature. This methodology is affordable as it uses minimal experimental testing and can be applied to any MOF materials to explore its suitability for practical applications.

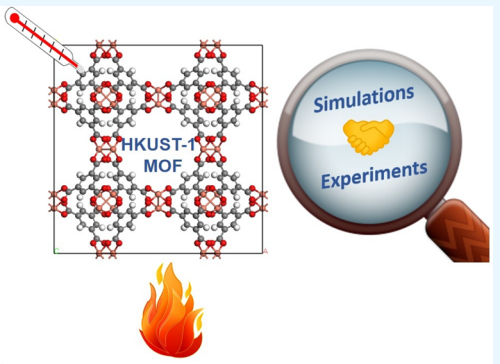

1. INTRODUCTION

The development of efficient porous materials for the adsorptive separation of a selected gas from a mixture is of supreme importance in recent times because of its relevance in industrial and environmental applications.[1−3] Among the various porous solids, metal−organic frameworks (MOFs), during the past two decades, offer various pore sizes,[4] shapes, and topologies[5] that can be suitable for CO_2 capture, making these solids exceptional candidates in the area of natural gas purification and flue gas treatment.[6−8] The highest reported gravimetric uptake of CO_2 is 27.5 wt % in MOF-74-Mg at 1 bar, at 298 K,[9] and 74.2 wt % at 50 bar, at 298 K, for MOF-200, respectively.[10] The best performers for CO_2/N_2 (15:85) selectivity are reported as 33.7[11,12] and 225 at 298 K[13] in UTSA-1 and MAF-66, respectively. Thermally robust MOFs are highly required for such applications.[14] For instance, one of the main methods of regenerating MOFs is the temperature swing adsorption (TSA), where the MOFs are heated to drive off the captured molecules.[15] Developing a stable MOF that can be regenerated multiple times is needed for practical applications.[14] Furthermore, capturing CO_2 directly from flue gas takes place usually at relatively high temperatures.[16,17]

The thermal stability of MOFs has been previously investigated by different experimental methods such as thermogravimetric analysis (TGA), differential scanning calorimetry (DSC), and in situ powder X-ray diffraction (PXRD).[18,19] Each method has its advantages and disadvantages. For example, TGA can provide information on mass loss at different atmospheres, while any changes in crystallographic phases can be missed, which can be captured by PXRD.[20] Also, DSC can provide clues on endothermic and exothermic processes while heating the material only. The thermal stability of MOFs can also be studied theoretically by performing molecular dynamics (MD)[21] and density functional theory (DFT).[22]

Here, we report a comprehensive methodology that combines theoretical and experimental analyses to investigate the thermal robustness of MOFs for CO_2 capture applications. The prototypical prevalent MOF, HKUST-1, was selected to examine the methodology owing to its easy synthesis, commercial availability in the gram scale, and promising porosity for CO_2 capture.[23,24] HKUST-1 was first synthesized by Chui et al.[25] and consists of 1,3,5-benzenetricarboxylate (BTC) linkers coordinated to Cu ions in a cubic lattice. Recently, Bin et al.[26] studied the thermal structural decomposition of HKUST-1 under air, hydrogen, and nitrogen using TGA analysis. They observed that the formation of

Received: August 20, 2022
Accepted: November 16, 2022
Published: December 8, 2022

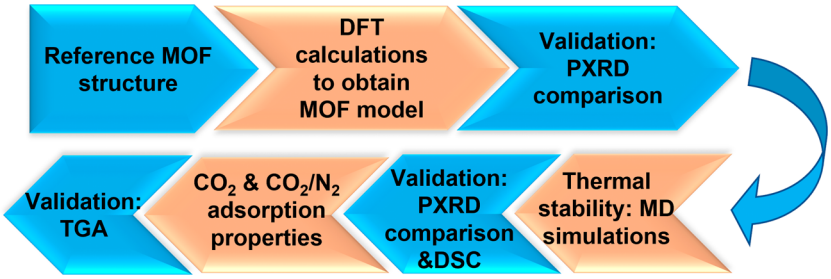

Figure 1. Schematic workflow that consists of a theoretical and experimental methodology. PXRD: powder X-ray diffraction. DSC: differential scanning calorimetry. TGA: thermogravimetric analysis. Blue and orange colors correspond to experimental and computational methodologies, respectively.

unsaturated metal centers while heating the sample to 350 °C triggers the instability in the MOF structure.

To our knowledge, this is the first report on proposing a generalized hybrid experimental and computational methodology to understand the thermal and adsorption properties of a MOF structure. The schematic of our workflow is shown in Figure 1. In this methodology, DFT calculations were performed to predict the structural model of the MOF, and it has been validated by comparing the calculated and experimental PXRD patterns. Further, temperature annealing of classical MD simulations was carried out to understand the thermal robustness in the structural model. The observations were validated with the in situ temperature-dependent PXRD data where the MOF was heated, and in situ PXRD patterns were being captured as a function of temperature to detect any possible phase transition at different atmospheric gases. Finally, the adsorption properties of the MOF were explored by calculating the single-component CO_2 and N_2 gases and the coadsorption of the CO_2/N_2 (0.15/0.85) mixture adsorption isotherms using GCMC simulations. The selectivity toward CO_2 gas was characterized using TGA under CO_2, N_2, and air while probing the mass variations of the MOF as a function of temperature.

2. COMPUTATIONAL METHODS

Detailed information about the density functional theory (DFT) calculations, force-field-based molecular dynamics (MD), and grand canonical Monte Carlo (GCMC) simulations can be found in the Supporting Information, Section S1. First, periodic DFT calculations were performed on an experimentally well-characterized HKUST-1[27] (lattice constants: $a = b = c = 26.304$ Å and $\alpha = \beta = \gamma = 90°$) to get a possible MOF structural model using PBE-D3 in CP2K.[28] The geometry and cell parameter optimized MOF structure was validated by comparing its PXRD with the experimental data.

Further, we performed computationally efficient empirical force field MD simulations at temperatures of 300−650 K to understand the microscopic insight of the thermal stability of HKUST-1, as the DFT-based optimization calculations can provide the structural details at 0 K. A well-developed UFF-FM (universal force field−flexible metal) force field that captures the flexibility of MOF structures was employed in LAMMPS.[29] An equilibrated 1 × 1 × 1 HKUST-1 structure was obtained from the following calculations: (i) geometry and cell parameter optimization, (ii) constant-NVT MD simulations, and (iii) subsequent constant-NPT MD simulations for 10 ns. The final modeled structure's PXRD was calculated using Mercury[30] at each temperature and compared against experiments.

Additionally, we attempted to study the adsorption and separation characteristics of HKUST-1 structures obtained at 300−650 K using GCMC simulations in the RASPA 2.0.47 version of code.[31] Single-component CO_2 and N_2, as well as their mixture in 0.15/0.85 mole fraction of adsorption isotherms, were calculated. We employed UFF[32] and DREIDING[33] force fields for the Cu metal atom and nonmetal atoms, respectively, and transferrable force fields for CO_2[34] and a three-site model for N_2.[35] Electrostatic interactions were computed based on the atomic charges obtained from the charge equilibration (Q_{eq}) method.[36]

3. EXPERIMENTAL METHODS

3.1. Synthesis and Characterization. All the chemicals used for this study were purchased from Sigma-Aldrich and used without further purification. The HKUST-1 was synthesized by following a reported typical synthesis process of mixing the copper nitrate trihydrate with benzene-1,3,5-tricarboxylic acid in water/ethanol (1:1) in a Teflon-coated autoclave at an elevated pressure at 100 °C for 24 h.[37]

To probe the structural thermal stability at variable temperatures, in situ powder X-ray diffraction (PXRD) and differential scanning calorimetry (DSC) were simultaneously performed using the Rigaku SmartLab system (Cu Kα 1.5404 Å). The sample was placed in a standard aluminum pan (0.9 × 0.9 × 0.2 mm^3) with another reference pan close to it in the same furnace. The measurement and reference samples were kept inside a closed silver lid to ensure thermal insulation. The whole furnace is surrounded by a thermally insulating cover with multiple gas ports for purging and venting, which allow uniform gas flow in the furnace. Three different atmospheric gases were introduced into the furnace: air, N_2, and CO_2 at a flow rate of 10 mL/min. The samples were heated to 513 K with a ramping rate of 5°/min. The sample was maintained at constant temperature values (each $T = 30$ K) and fixed time intervals (30 min) to ensure stable conditions for obtaining PXRD patterns.

Figure S1a shows the PXRD pattern at room temperature, confirming the existence of the single phase of HKUST-1 with cubic crystal structure and symmetry space group of $Fm\bar{3}m$.[27] The specific surface area of prepared HKUST-1 was measured by a nitrogen adsorption/desorption isotherm in a liquid nitrogen atmosphere ($T = 77$ K) with a Micromeritics ASAP 2020 BET N_2 (Norcross, GA, U.S.A.) surface area analyzer (see Figure S1b). The surface area was determined using the Brunauer−Emmett−Teller (BET) method. Before the surface area measurement, the sample degassing was carried out at 250 °C under vacuum for 8 h. The specific surface area obtained by

https://doi.org/10.1021/acsomega.2c05345
ACS Omega 2022, 7, 46515−46523

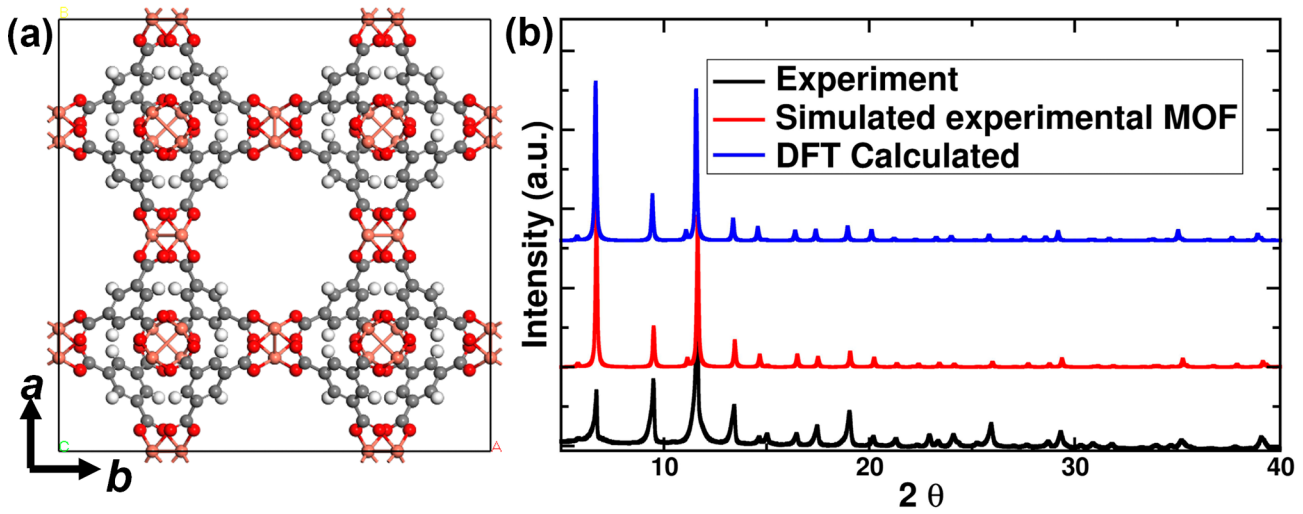

Figure 2. (a) Ball and stick representation of the DFT-based optimized configuration of the HKUST-1 MOF. Color scheme: C, gray; H, white; Cu, pink; and O, red. (b) Blue color curve: DFT calculated structure's PXRD pattern. Red color curve: the simulated PXRD pattern that is obtained from the theoretical model of the experimental desolvated structure, HKUST-1. Black curve represents the experimental PXRD data.

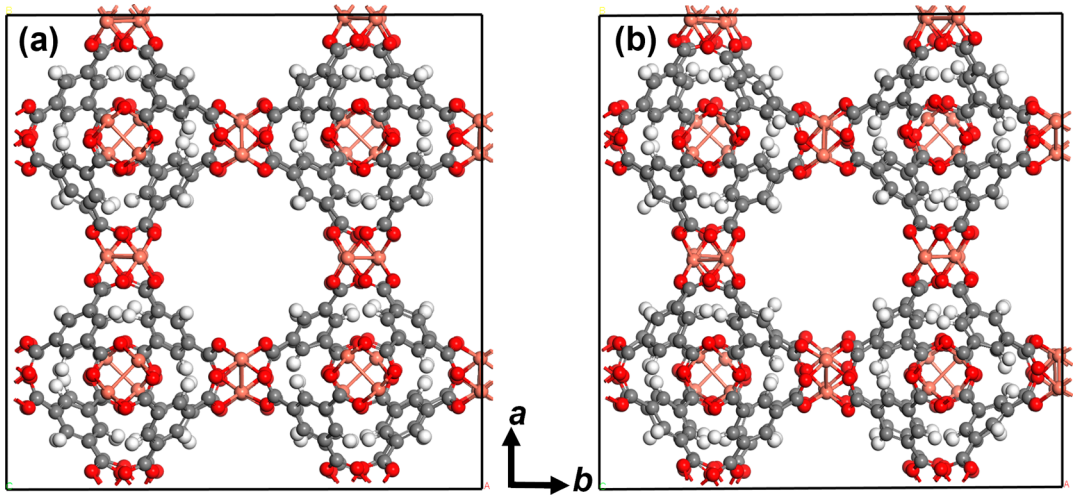

Figure 3. (a) and (b) Molecular dynamics snapshots of HKUST-1 at 300 and 650 K, respectively. Color scheme: C, gray; H, white; Cu, pink; and O, red.

BET (1453 m^2/g) of HKUST-1 is comparable to the previously reported value.[37]

3.2. Thermogravimetric Analysis. To investigate the thermal stability and the understanding of CO_2 selectivity in HKUST-1, thermogravimetric analysis (TGA) was performed using TA Instruments (ADT600). HKUST-1 (~6.5 mg) was placed in an alumina crucible underflow of CO_2 gas (20−30 mL/min) at a heating rate of 5 °C/min from room temperature to 60 °C. The temperature was held at 60 °C for 3 h and then ramped up to 300 °C at a rate of 5 °C/min. Similar experimental conditions were applied under two separate atmospheres of air and N_2. Additional lab piping hoses have been installed to the TGA setup to ensure the safe release of CO_2 out of the TGA furnace through the in-house exhaust system.

4. RESULTS AND DISCUSSION

4.1. Structural Prediction. Periodic density functional theory calculations were performed to obtain the possible MOF structural model, which is relevant to the experimentally measured PXRD pattern as mentioned in Section S1.1 and Section 2. A reference structure, HKUST-1, MOF[17] was taken as a guess framework structure that could be relevant to experimental synthetic conditions. A cubic simulation cell consisting of a 1 × 1 × 1 unit cell was considered with crystallographic parameters $a = b = c = 26.304$ Å and $\alpha = \beta = \gamma = 90°$. The geometry and cell parameters of the desolvated MOF structure (all solvent removed) were optimized using DFT calculations, as discussed in Section S1.1 and Section 2. The volume of the optimized structure has a 1.9% difference from the reference structure, which shows the adaptability of the PBE-D3 method to the MOF structure. The resultant structural model is shown along the *c*-axis in Figure 2a. A PXRD pattern of the modeled MOF structure was calculated and compared to the experimental data to validate the structural model. A PXRD pattern was obtained using Mercury.[30] The comparison of PXRD patterns is shown in Figure 2b. A good agreement between the calculated and simulated pattern obtained from the theoretical model for the experimental structure validates our modeled MOF structure that has the equivalent framework structure of HKUST-1.[27]

https://doi.org/10.1021/acsomega.2c05345
ACS Omega 2022, 7, 46515−46523

The first peak intensity at 2θ of 6° is higher in the calculated and simulated pattern when compared to experimental data and could be related to the experimental sample quality and the stress/strain experiences in each polycrystalline phase while preparing the powder sample for the measurement. The calculations consist of an ideal clean solvent removed structure.

To further delineate the microscopic insight into the thermal structural stability of the HKUST-1 model, force-field-based MD simulations were performed, and the details of the simulations are provided in Section S1.2. The theoretical observations were validated with the in situ PXRD and DSC results that were measured at different temperatures, as mentioned in Section 3.1.

4.2. Structural Dynamics. The DFT-modeled structure is further subjected to study of its thermal stability at temperatures of 300−650 K using computationally viable force field-based simulations. UFF-FM force fields were considered to model MOF structure. This force field was well studied to reproduce the elastic properties of MOFs.[38] Both geometry and cell parameters of HKUST-1 were optimized to check the adaptability of the force field on the MOF. The PXRD pattern of the force-field-based optimized structure was compared to the data obtained for the DFT calculated structure as shown in Figure S2. A good agreement of PXRD patterns between force field and DFT calculations validates the perfect adaptability of the UFF-FM force field on our modeled structure. Therefore, we used these potential parameters for further simulations.

Constant-NPT MD simulations were performed at 300−650 K. MOF structure was equilibrated at 10 ns at each temperature. The resultant MOF configuration at each temperature was characterized using PXRD patterns that were calculated using Mercury.[30] Snapshots of the equilibrated HKUST-1 structures obtained at 300 and 650 K are shown in Figure 3a and 3b.

The calculated PXRD pattern is compared to the available experimental patterns to further validate the calculations. As per Figure 3a and 3b, the MOF structure almost maintains its structural integrity from 300 to 650 K, and this observation is reflected in the unchanged PXRD patterns at these temperatures. Details of the experimental measurements are mentioned in the following text.

In situ PXRD and consequent DSC were carried out at different temperatures and atmospheric gases to understand the thermal propensity of HKUST-1. The methodology of the experimental setup is described in Section 3.1. Figure 4a shows the DSC results for HKUST-1 at different temperatures and atmospheric gases. The temperature was increased at multiple heating steps (every 30 K) up to 513 K, and then it was cooled to room temperature with similar temperature steps. It is worth noting that endothermic (sharp) peaks in the green and blue curves of Figure 4a appear when the heating starts, from T = 300 to 330 K and T = 330 to 360 K (from 30 min to 2 h), due to the existence of H_2O molecules that did not evaporate yet from HKUST-1.[37] While heating HKUST-1 to 330 K, DSC shows higher endothermic heat flow in the air or N_2 atmosphere (gray line in Figure 4a) than in CO_2. This phenomenon could be explained as CO_2 molecules assisting, in parallel with heat, in dehydrating HKUST-1 faster due to its higher affinity to capture CO_2. On the other hand, the dehydration of HKUST-1 would require higher heat in N_2 or air, and hence larger DSC peaks are observed at the heating step toward 330 K. This phenomenon discloses the dehydration in the HKUST-1 competitively faster in the presence of CO_2 than air or N_2 adsorption. In addition, the temperature was held for 30 min at each DSC step to obtain a PXRD pattern, as shown in Figure 4b. In all heating and cooling intervals, the crystal structure of HKUST-1 is preserved without prominent changes in its crystal phase, as confirmed by the PXRD patterns in Figure 4b.

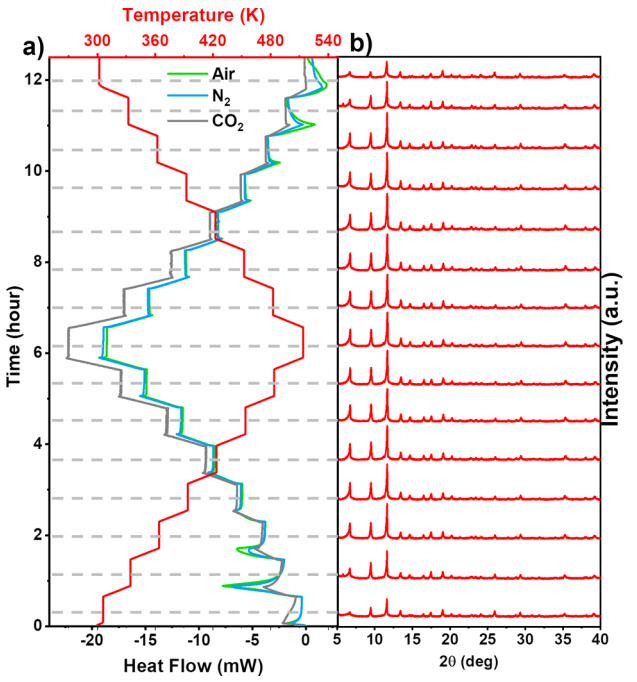

Figure 4. In situ (a) differential scanning calorimetry (DSC) and (b) powder X-ray diffraction (PXRD) were performed simultaneously under three different atmospheres (air, N_2, and CO_2). The samples retain their phase structure as confirmed by PXRD taken at each heating interval (horizontal gray lines in (a)).

A complete comparison between the experimental and calculated PXRD patterns is shown in Figure S3. The solid curve in Figure S3 represents the calculated PXRD patterns of MOF structures obtained from force-field-based MD simulations, whereas dotted curves represent the corresponding experimental PXRD. Good quantitative agreement between calculated and experimental PXRD patterns discloses that the modeled structures are the possible structural models consistent with the experimental observations at different temperatures. In addition, in terms of the force field, the UFF-FM potentials are also well suited to model HKUST-1 at higher temperatures.

We have also examined the effect of temperature on the structural properties of HKUST-1. We carried out force-field-based temperature annealing and quenching MD simulations; i.e., the temperature was gradually increased starting with 300−650 K in annealing MD simulations, and the temperature was cooled in reverse order from 650 to 300 K in the later MD simulations. At each temperature, the system was equilibrated for 10 ns. The changes in simulation cell volume and parameters while heating and cooling the MOF structure are shown in Figures 5a,b. The volume and lattice parameters of the HKUST-1 unit cell decreased with temperature. While cooling the MOF structure, all the volume and cell parameters returned to the initial configuration in a completely reversible process. A similar trend in the averaged lattice constants with increasing temperature was observed in air, CO_2, and N_2 environments, experimentally based on in situ PXRD patterns

https://doi.org/10.1021/acsomega.2c05345
ACS Omega 2022, 7, 46515−46523

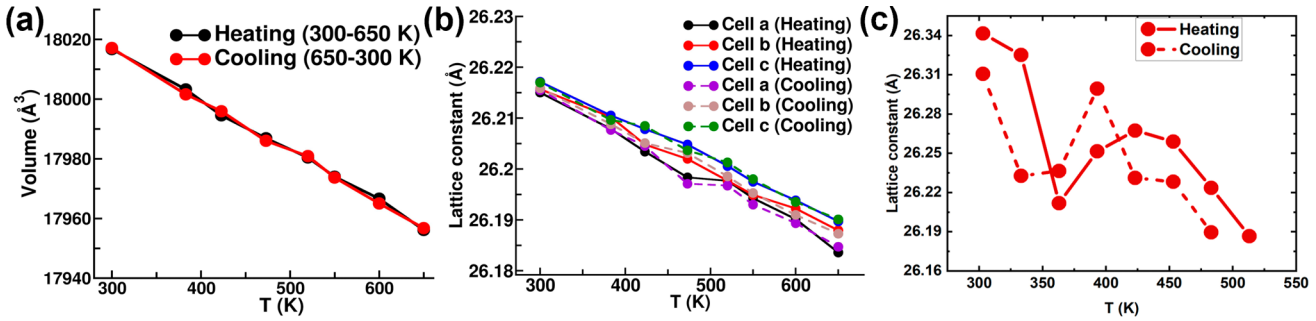

Figure 5. (a) Unit cell volume changes upon heating and cooling of the HKUST-1 MOF and (b) lattice constant, *a*, *b*, and *c*, changes upon heating and cooling of the MOF structure, respectively. (c) Averaged experimental lattice constants measured at CO_2, N_2, and air atmospheric conditions as a function of temperature.

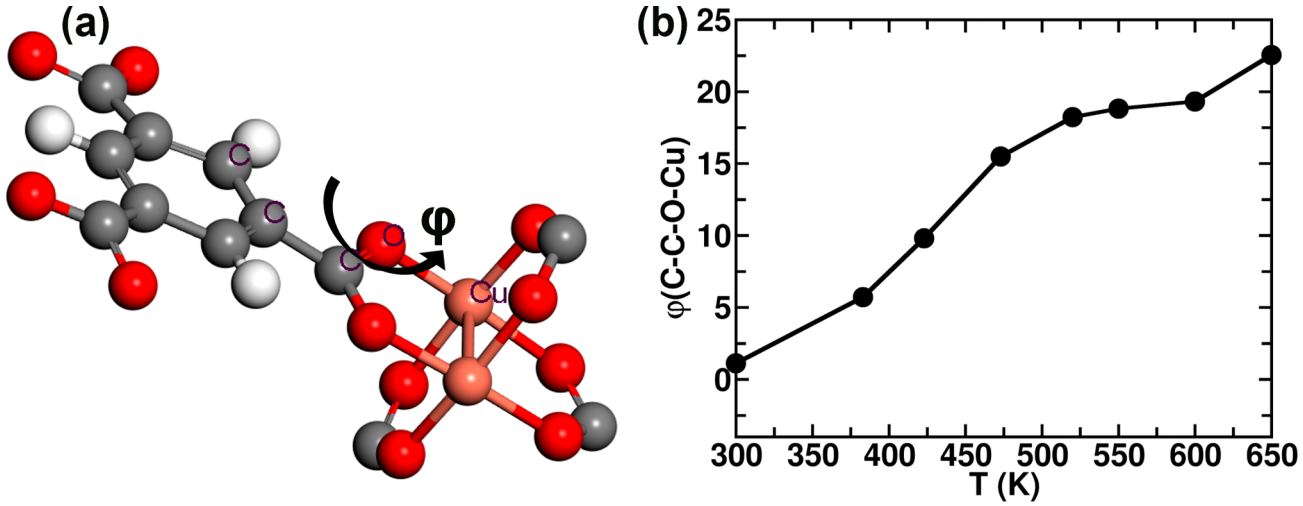

Figure 6. (a) Fragment of the Cu-metal node connected to the BTC linker that discloses the dihedral information on the C−C−C−O and C−C−O−Cu of the BTC linker and node. (b) Variations in the dihedral angle of C−C−O atom BTC linkers and the Cu atom of the metal node. Color scheme: C, gray; H, white; Cu, pink; and O, red.

shown in Figure 5c. The original data of the lattice constant measured at air, CO_2, and N_2 conditions are shown in Figure S4. Due to considerably fewer variations in the lattice constant at different experimental conditions, we took the average to compare with the calculations. The qualitative agreement between the calculated and experimental lattice constant variation further provided confidence in the simulation model.

The unusual phenomenon of volume contraction upon heating is referred to as negative thermal expansion (NTE). To obtain a microscopic understanding of the NTE behavior in HKUST-1, the dihedral angles between the carboxyl bond of the benzene-1,3,5-tricarboxylate (BTC) linker connected to the Cu were analyzed for the equilibrated configuration from the MD trajectory. A linker tilting behavior was observed while increasing the temperature.

A dihedral angle is φ (C−C−O−Cu: where C−C−O atoms correspond to the BTC linker and Cu atoms belong to the Cu-metal node), calculated to get the interlinked flexibility. The schematic representation of the φ is shown in Figure 6a. The variations in φ are directly proportional to temperature, as shown in Figure 6b. This analogous structural variation around the Cu-paddle wheel node allows the organic linker, BTC, to bend, deform, or shear between the Cu nodes and BTC linkers because of the relatively weak coordination bonds. Hence, the tilting flexibility of BTC linkers around the rigid metal cluster is responsible for the anomalous thermal expansion of HKUST-1. PXRD patterns, which are shown in Figure 4, could not capture these subtle changes in the structure as the PXRD experiments see only the time-averaged structures that retain the symmetry; therefore, no significant differences were observed in the PXRD patterns with temperature changes. However, the subtle structural changes can be visually reflected in the MD simulation snapshots obtained at 300 and 650 K, as shown in Figure 3a and 3b. To support our observations, similar kinds of studies were reported by Sang et al. for MOF-C6, MOF-C10, MOF-C16, MOF-C22, and MOF-C30, where they observed a Zn_4O cluster rotation with increasing temperature that causes the NTE in the structures.[39]

The adsorption properties of HKUST-1 were studied to understand its CO_2 storage and selectivity from flue gases using GCMC simulations. All the simulation details are described in Section S1.3 and Section 2.

4.3. Adsorption Isotherms. The validated structural models were further used to calculate CO_2 and N_2 adsorption isotherms at 300 K and to compare our results with the available experimental data.[40] We calculated CO_2 and N_2 adsorption isotherms in six different HKUST-1 structures that were obtained from various simulation conditions: (i) MOF structure with the literature-reported structure (reference MOF), (ii) DFT-based optimized MOF structure, and (iii) MOF structure obtained at 300 K (named as 300 K-MOF), (iv) at 383 K (383 K-MOF), (v) at 423 K (423 K-

https://doi.org/10.1021/acsomega.2c05345
ACS Omega 2022, 7, 46515−46523

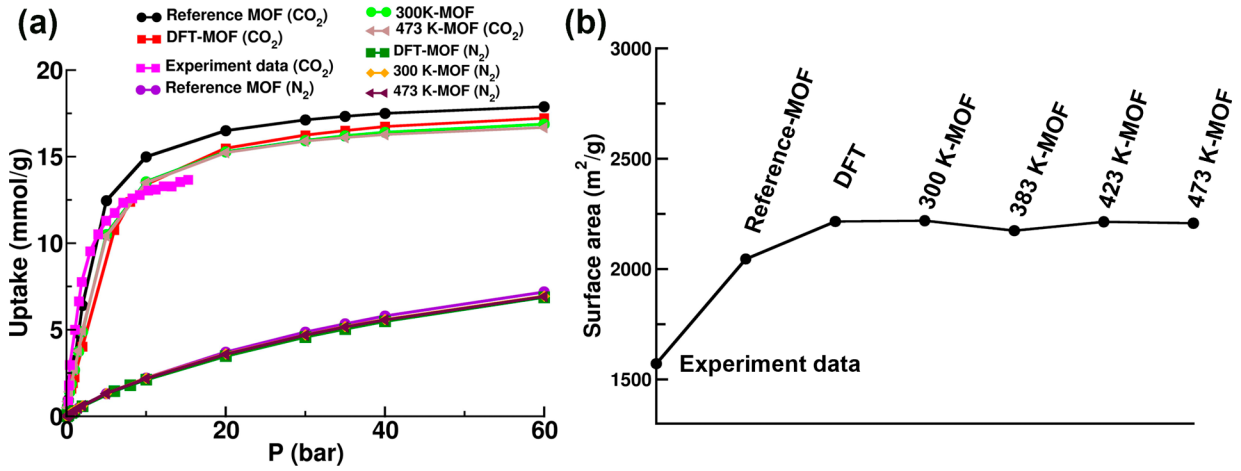

Figure 7. (a) Adsorption isotherms of CO_2 and N_2 at 300 K in the structures obtained at different temperatures and comparison concerning experimental data.[40] The experimental adsorption data of N_2 are not available at 300 K; hence, it is not mentioned in the plot. (b) Surface area comparison between calculated structures and the experimental data obtained from the N_2 adsorption isotherm at 77 K. The nomenclature follows temperature (K)-MOF structure for the reader's clarity on the structure's thermal conditions.

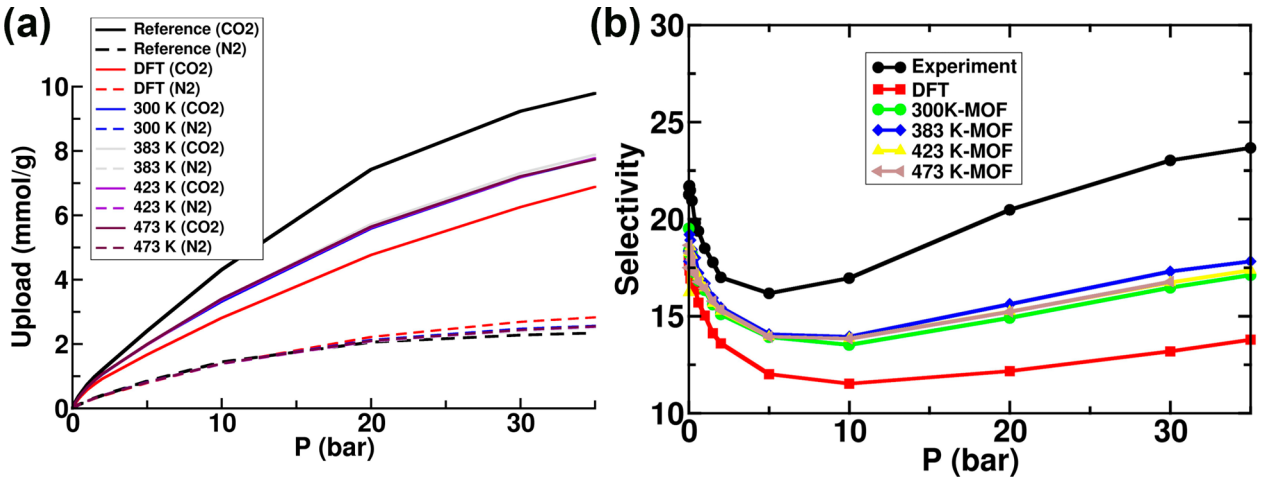

Figure 8. (a) Co-adsorption isotherm of CO_2/N_2 (0.15/0.85 mole fraction) at 300 K in the structures obtained at different temperature conditions. Here are the labeled temperatures that are not used in GCMC simulations. Their notation gives clarity to the readers that the MOF structure was obtained at the mentioned temperature. (b) Selectivity of CO_2 over N_2 in the CO_2/N_2 mixture.

MOF), and (vi) at 473 K (473 K-MOF) using force-field-based MD simulations. The resultant single-component CO_2 and N_2 adsorption isotherms at 300 K are shown in Figure 7a and Figure S5.

We compared the calculated CO_2 adsorption isotherms with the experimentally reported adsorption data (available up to 15 bar) in HKUST-1 by Liang et al.[40] The calculated saturation CO_2 uptake obtained was 10% more than that from the experimental data. To understand the deviation in the amount of CO_2 uptake, we further examined the geometrical characteristics and surface area in the calculated structure and compared them to the experimentally measured quantity. A simple geometric approach that consists of a N_2 probe with a diameter of 3.86 Å was rolled over the MOF structure, and the accessible surface area was calculated using Monte Carlo integration with the Zeo++ package.[41] The comparison between the calculated surface area of different modeled structures and the experimentally measured value obtained from N_2 adsorption isotherms at 77 K is shown in Figure 7b. The calculated surface area was 20% higher than the experimental value. This difference may be attributed to the poorly experimentally activated samples, whereas in our GCMC simulations, the pure structure was considered. Hence, as a result, the CO_2 uptake was calculated to be 10% higher than the experimental data.

4.4. Separation of the CO_2/N_2 Mixture. In separation processes, a good indication of the separation ability consists of estimating the selectivity of a MOF material. The following expression defines the selectivity (S) for CO_2 over N_2: $S(CO_2/N_2) = (x_{CO2}/x_{N2})(y_{CO2}/y_{N2})$, where x_{CO2} and x_{N2} are the mole fractions of CO_2 and N_2 in the adsorbed phase, respectively, while y_{CO2} and y_{N2} are the mole fractions of CO_2 and N_2 in the bulk phase, respectively. We calculated the selectivities from the coadsorption isotherms for CO_2/N_2 from their 0.15/0.85 mole fraction gas mixture in the MOF structures obtained from the constant-NPT MD simulations. The mixture of CO_2/N_2 coadsorption isotherms and the calculated selectivity of CO_2 over N_2 are shown in Figure 8a and 8b.

Solid curves in Figure 8a correspond to CO_2 adsorption uptake, and a dotted line with the same color as the solid line corresponds to the N_2 uptake. In all different MOF structures, CO_2 shows a higher uptake than N_2. This is due to the higher

https://doi.org/10.1021/acsomega.2c05345
ACS Omega 2022, 7, 46515−46523

polarizability of CO_2 providing favorable interactions with the MOF atoms, thus resulting in the higher tendency to get adsorbed in the MOF framework. This tendency of HKUST-1 toward adsorbing CO_2 is also corroborated by the experimental DSC, as discussed previously (Figure 4a). A similar phenomenon in the selectivity calculations is shown in Figure 7b. At lower pressures (zero loading), CO_2 has a selectivity value of 20, which is in good agreement with the experimentally reported value of 19 by Muhammad et al.[42] At higher pressures, the selectivity varies due to the competitive adsorption between N_2 and CO_2 in the HKUST-1.

To further validate the CO_2 selectivity from the CO_2/N_2 mixture experimentally, an affordable TGA experiment was carried out in the presence of CO_2, N_2, and air environments. The experimental setup for these measurements is mentioned in Section 3.2.

4.5. Thermogravimetric Analysis. The TGA analysis of weight loss as a function of time and temperature under an air, N_2, and CO_2 atmosphere is shown in Figure 9. The sample was

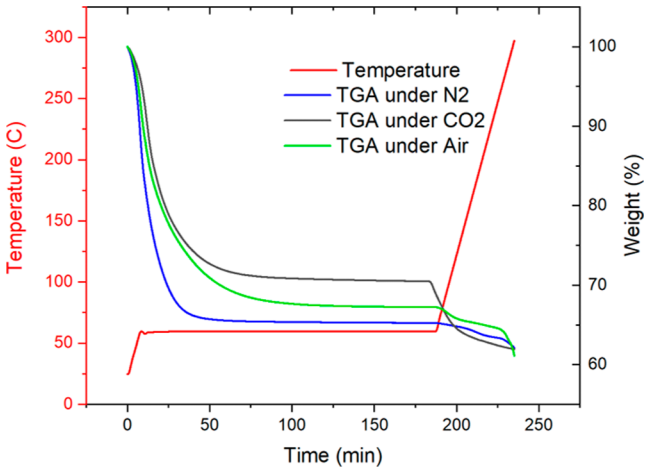

Figure 9. Thermogravimetric analysis of HKUST-1 done in N_2, CO_2, and air.

heated to 60 °C for 3 h, where HKUST-1 has lost 33% (black curve), 35% (blue curve), and 30% (green curve) of its initial weight. This loss is attributed to the removal of the surface water.[37] As HKUST-1 is heated from 60 to 300 °C, a weight loss of 10% is related to the removal of metal-coordinated water molecules.[43] At T = 60 °C, three prominent features distinguish the TGA data for HKUST-1 in the three different atmospheres. First, the weight loss is the least in CO_2, which could be related to the selectivity of capturing CO_2, which assisted in compensating for the weight loss caused by the evaporated water. This result is supported by our calculations (Figures 7a and 8) and the DSC results where higher heat flow was noticed due to CO_2 capture (see Figure 4a). On the other hand, TGA in still air showed higher weight loss compared to the experiment in CO_2. Finally, the weight loss is the highest in the case of N_2, which could be attributed to the dehydration driven by the kinetic energy of the flowing N_2 molecules.

5. CONCLUSION

We propose a computational and experimental methodology that allows a cost and time-effective assessment of the thermal robustness and adsorption capabilities of porous materials. A MOF model that is quantitatively consistent with experimental PXRD was obtained from DFT calculations. Further, its thermal stability was characterized by the computationally viable classical MD simulations, and the calculated PXRD of the resultant structural models are in good agreement with the experimental DSC and consequent in situ PXRD data. Using a computational microscopic investigation, the negative thermal expansion in the HKUST-1 could be explained by an increased distortion in the dihedral angle of weak linker and metal bonds. Additionally, a single gas component and binary mixture of CO_2 and N_2 adsorption isotherm calculations using GCMC simulations offer an affordable and time-effective study of the HKUST-1 selectively to adsorb CO_2 from the postcombustion flue gas. Gas selectivity experiments are time-consuming and require capital costs to acquire and operate costly equipment. Our theoretical selectivity observations were validated with the experimental DSC and TGA analysis. According to DSC characterization, the higher endothermic heat flow and the lower weight loss in TGA analysis in the presence of a CO_2 environment validate the CO_2-selective adsorption tendency more than N_2 or air. Our proposed methodology minimizes the experimental investigations and substitutes it with a liable calculation, thus democratizing the assessment of thermal robustness of metal−organic frameworks and speeding up the timeline for their development and use in practical applications.

■ ASSOCIATED CONTENT

Supporting Information

The Supporting Information is available free of charge at https://pubs.acs.org/doi/10.1021/acsomega.2c05345.

Comparison of the experimental and reference XRD pattern of HKUST-1 and the experimental N_2 adsorption isotherm at 77 K; details of the DFT calculations, force-field MD simulations, GCMC simulations; additional figures such as a comparison between DFT calculated and experimental PXRD patterns; comparison of the experimental and calculated PXRD patterns of the MOF structures obtained at different temperatures; the experimental lattice constant as a function of temperature at CO_2, N_2, and air atmospheric conditions; and single-component adsorption of CO_2 and N_2 at 300 K in HKUST-1 (PDF)

■ AUTHOR INFORMATION

Corresponding Author

Fedwa El-Mellouhi − *Qatar Environment and Energy Research Institute, Hamad Bin Khalifa University, Doha, Qatar*; orcid.org/0000-0003-4338-9290; Email: felmellouhi@hbku.edu.qa

Authors

Satyanarayana Bonakala − *Qatar Environment and Energy Research Institute, Hamad Bin Khalifa University, Doha, Qatar*

Anas Abutaha − *Qatar Environment and Energy Research Institute, Hamad Bin Khalifa University, Doha, Qatar*

Palani Elumalai − *Qatar Environment and Energy Research Institute, Hamad Bin Khalifa University, Doha, Qatar*

Ayman Samara − *Qatar Environment and Energy Research Institute, Hamad Bin Khalifa University, Doha, Qatar*

https://doi.org/10.1021/acsomega.2c05345
ACS Omega 2022, 7, 46515−46523

Said Mansour − *QEERI, Core Labs, Qatar Environment & Energy Res Inst, Doha, Qatar;* orcid.org/0000-0001-9091-4276

Complete contact information is available at: https://pubs.acs.org/10.1021/acsomega.2c05345

Notes

The authors declare no competing financial interest.

■ ACKNOWLEDGMENTS

This work is financially supported by Qatar National Research Fund, QNRF NPRP12C, and NOMDEE. The authors thank Hamad Bin Khalifa University for providing HPC resources, Hazeem. We thank Dr. Abdulkarem I. Amhamed for his valuable suggestions. We thank Dr. Kamal Mroue for the helpful discussions.

■ REFERENCES

(1) Cadiau, A.; Belmabkhout, Y.; Adil, K.; Bhatt, P. M.; Pillai, R. S.; Shkurenko, A.; Martineau-Corcos, C.; Maurin, G.; Eddaoudi, M. Hydrolytically Stable Fluorinated Metal-Organic Frameworks for Energy-Efficient Dehydration. *Science* **2017**, *356* (6339), 731−735.

(2) Akiyama, G.; Matsuda, R.; Sato, H.; Hori, A.; Takata, M.; Kitagawa, S. Effect of Functional Groups in MIL-101 on Water Sorption Behavior. *Microporous Mesoporous Mater.* **2012**, *157*, 89−93.

(3) Chavan, S.; Vitillo, J. G.; Larabi, C.; Alessandra Quadrelli, E.; Dietzel, P. D. C.; Bordiga, S. Functionalization of CPO-27-Ni through Metal Hexacarbonyls: The Role of Open Ni2+ Sites. *Microporous Mesoporous Mater.* **2012**, *157*, 56−61.

(4) Keskin, S.; van Heest, T. M.; Sholl, D. S. Can Metal−Organic Framework Materials Play a Useful Role in Large-Scale Carbon Dioxide Separations? *ChemSusChem* **2010**, *3* (8), 879−891.

(5) Li, J.-R.; Ma, Y.; McCarthy, M. C.; Sculley, J.; Yu, J.; Jeong, H.-K.; Balbuena, P. B.; Zhou, H.-C. Carbon Dioxide Capture-Related Gas Adsorption and Separation in Metal-Organic Frameworks. *Coord. Chem. Rev.* **2011**, *255* (15), 1791−1823.

(6) Pillai, R. S.; Benoit, V.; Orsi, A.; Llewellyn, P. L.; Wright, P. A.; Maurin, G. Highly Selective CO2 Capture by Small Pore Scandium-Based Metal−Organic Frameworks. *J. Phys. Chem. C* **2015**, *119* (41), 23592−23598.

(7) Barea, E.; Turra, F.; Rodriguez Navarro, J. A. Separation and Purification of Gases by MOFs. *Metal-Organic Frameworks* **2011**, 69−97.

(8) Duan, J.; Jin, W.; Krishna, R. Natural Gas Purification Using a Porous Coordination Polymer with Water and Chemical Stability. *Inorg. Chem.* **2015**, *54* (9), 4279−4284.

(9) Bao, Z.; Yu, L.; Ren, Q.; Lu, X.; Deng, S. Adsorption of CO2 and CH4 on a Magnesium-Based Metal Organic Framework. *J. Colloid Interface Sci.* **2011**, *353* (2), 549−556.

(10) Furukawa, H.; Ko, N.; Go, Y. B.; Aratani, N.; Choi, S. B.; Choi, E.; Yazaydin, A. Ö.; Snurr, R. Q.; O'Keeffe, M.; Kim, J.; Yaghi, O. M. Ultrahigh Porosity in Metal-Organic Frameworks. *Science (80-.)* **2010**, *329* (5990), 424−428.

(11) Xiong, S.; Gong, Y.; Wang, H.; Wang, H.; Liu, Q.; Gu, M.; Wang, X.; Chen, B.; Wang, Z. A New Tetrazolate Zeolite-like Framework for Highly Selective CO2/CH4 and CO2/N2 Separation. *Chem. Commun.* **2014**, *50* (81), 12101−12104.

(12) Xiang, S.; He, Y.; Zhang, Z.; Wu, H.; Zhou, W.; Krishna, R.; Chen, B. Microporous Metal-Organic Framework with Potential for Carbon Dioxide Capture at Ambient Conditions. *Nat. Commun.* **2012**, *3* (1), 954.

(13) Lin, R.-B.; Chen, D.; Lin, Y.-Y.; Zhang, J.-P.; Chen, X.-M. A Zeolite-Like Zinc Triazolate Framework with High Gas Adsorption and Separation Performance. *Inorg. Chem.* **2012**, *51* (18), 9950−9955.

(14) Voskanyan, A. A.; Goncharov, V. G.; Novendra, N.; Guo, X.; Navrotsky, A. Thermodynamics Drives the Stability of the MOF-74 Family in Water. *ACS Omega* **2020**, *5* (22), 13158−13163.

(15) Mason, J. A.; Sumida, K.; Herm, Z. R.; Krishna, R.; Long, J. R. Evaluating Metal−Organic Frameworks for Post-Combustion Carbon Dioxide Capture via Temperature Swing Adsorption. *Energy Environ. Sci.* **2011**, *4* (8), 3030−3040.

(16) Barea, E.; Turra, F.; Rodriguez Navarro, J. A. Separation and Purification of Gases by MOFs. *Metal-Organic Frameworks* **2011**, 69−97.

(17) Puccini, M.; Stefanelli, E.; Seggiani, M.; Vitolo, S. Removal of CO2 from Flue Gas at High Temperature Using Novel Porous Solids. *Chem. Eng. Trans.* **2016**, *47*, 139−144.

(18) Healy, C.; Patil, K. M.; Wilson, B. H.; Hermanspahn, L.; Harvey-Reid, N. C.; Howard, B. I.; Kleinjan, C.; Kolien, J.; Payet, F.; Telfer, S. G.; Kruger, P. E.; Bennett, T. D. The Thermal Stability of Metal-Organic Frameworks. *Coord. Chem. Rev.* **2020**, *419*, 213388.

(19) Pan, C.; Nan, J.; Dong, X.; Ren, X.-M.; Jin, W. A Highly Thermally Stable Ferroelectric Metal−Organic Framework and Its Thin Film with Substrate Surface Nature Dependent Morphology. *J. Am. Chem. Soc.* **2011**, *133* (32), 12330−12333.

(20) Xin, C.; Ren, Y.; Zhang, Z.; Liu, L.; Wang, X.; Yang, J. Enhancement of Hydrothermal Stability and CO2 Adsorption of Mg-MOF-74/MCF Composites. *ACS Omega* **2021**, *6* (11), 7739−7745.

(21) Mohamed, S. A.; Chong, S.; Kim, J. Thermal Stability of Methyl-Functionalized MOF-5. *J. Phys. Chem. C* **2019**, *123* (49), 29686−29692.

(22) Kharissova, O. V.; Kharisov, B. I.; González, L. T. Recent Trends on Density Functional Theory−Assisted Calculations of Structures and Properties of Metal−Organic Frameworks and Metal−Organic Frameworks-Derived Nanocarbons. *J. Mater. Res.* **2020**, *35* (11), 1424−1438.

(23) Du, J.; Zhou, C.; Yang, Z.; Cheng, J.; Shen, Y.; Zeng, X.; Tan, L.; Dong, L. Conversion of Solid Cu2(OH)2CO3 into HKUST-1 Metal-Organic Frameworks: Toward an under-Liquid Superamphiphobic Surface. *Surf. Coat. Technol.* **2019**, *363*, 282−290.

(24) Min Wang, Q.; Shen, D.; Bülow, M.; Ling Lau, M.; Deng, S.; Fitch, F. R.; Lemcoff, N. O.; Semanscin, J. Metallo-Organic Molecular Sieve for Gas Separation and Purification. *Microporous Mesoporous Mater.* **2002**, *55* (2), 217−230.

(25) Chui, S. S.-Y.; Lo, S. M.-F.; Charmant, J. P. H.; Orpen, A. G.; Williams, I. D. A Chemically Functionalizable Nanoporous Material [Cu3(TMA)2(H2O)3]N. *Science (80-.)* **1999**, *283* (5405), 1148−1150.

(26) Chen, B.; Zeng, X.; Liu, Y.; Xiao, F.; Huang, M.; Bing Tan, K.; Cai, D.; Huang, J.; Zhan, G. Thermal Decomposition Kinetics of M−BTC (M = Cu, Co, Zn, and Ce) and M−BTC/Pt Composites under Oxidative and Reductive Environments. *Chem. Eng. J.* **2022**, *450*, 138470.

(27) Yakovenko, A. A.; Reibenspies, J. H.; Bhuvanesh, N.; Zhou, H.-C. Generation and Applications of Structure Envelopes for Porous Metal−Organic Frameworks. *J. Appl. Crystallogr.* **2013**, *46* (2), 346−353.

(28) Kühne, T. D.; Iannuzzi, M.; Del Ben, M.; Rybkin, V. V.; Seewald, P.; Stein, F.; Laino, T.; Khaliullin, R. Z.; Schütt, O.; Schiffmann, F.; Golze, D.; Wilhelm, J.; Chulkov, S.; Bani-Hashemian, M. H.; Weber, V.; Borštnik, U.; Taillefumier, M.; Jakobovits, A. S.; Lazzaro, A.; Pabst, H.; Müller, T.; Schade, R.; Guidon, M.; Andermatt, S.; Holmberg, N.; Schenter, G. K.; Hehn, A.; Bussy, A.; Belleflamme, F.; Tabacchi, G.; Glöß, A.; Lass, M.; Bethune, I.; Mundy, C. J.; Plessl, C.; Watkins, M.; VandeVondele, J.; Krack, M.; Hutter, J. CP2K: An Electronic Structure and Molecular Dynamics Software Package - Quickstep: Efficient and Accurate Electronic Structure Calculations. *J. Chem. Phys.* **2020**, *152* (19), 194103.

(29) Plimpton, S. Fast Parallel Algorithms for Short-Range Molecular Dynamics. *J. Comput. Phys.* **1995**, *117* (1), 1−19.

(30) Macrae, C. F.; Sovago, I.; Cottrell, S. J.; Galek, P. T. A.; McCabe, P.; Pidcock, E.; Platings, M.; Shields, G. P.; Stevens, J. S.; Towler, M.; Wood, P. A. Mercury 4.0: From Visualization to Analysis, Design and Prediction. *J. Appl. Crystallogr.* **2020**, *53* (1), 226−235.

(31) Dubbeldam, D.; Calero, S.; Ellis, D. E.; Snurr, R. Q. RASPA: Molecular Simulation Software for Adsorption and Diffusion in Flexible Nanoporous Materials. *Mol. Simul.* **2016**, *42* (2), 81−101.
(32) Rappe, A. K.; Casewit, C. J.; Colwell, K. S.; Goddard, W. A.; Skiff, W. M. UFF, a Full Periodic Table Force Field for Molecular Mechanics and Molecular Dynamics Simulations. *J. Am. Chem. Soc.* **1992**, *114* (25), 10024−10035.
(33) Mayo, S. L.; Olafson, B. D.; Goddard, W. A. DREIDING: A Generic Force Field for Molecular Simulations. *J. Phys. Chem.* **1990**, *94* (26), 8897−8909.
(34) García-Sánchez, A.; Ania, C. O.; Parra, J. B.; Dubbeldam, D.; Vlugt, T. J. H.; Krishna, R.; Calero, S. Transferable Force Field for Carbon Dioxide Adsorption in Zeolites. *J. Phys. Chem. C* **2009**, *113* (20), 8814−8820.
(35) Martín-Calvo, A.; García-Pérez, E.; García-Sánchez, A.; Bueno-Pérez, R.; Hamad, S.; Calero, S. Effect of Air Humidity on the Removal of Carbon Tetrachloride from Air Using Cu−BTC Metal−Organic Framework. *Phys. Chem. Chem. Phys.* **2011**, *13* (23), 11165−11174.
(36) Rappe, A. K.; Goddard, W. A. Charge Equilibration for Molecular Dynamics Simulations. *J. Phys. Chem.* **1991**, *95* (8), 3358−3363.
(37) Al-Janabi, N.; Hill, P.; Torrente-Murciano, L.; Garforth, A.; Gorgojo, P.; Siperstein, F.; Fan, X. Mapping the Cu-BTC Metal−Organic Framework (HKUST-1) Stability Envelope in the Presence of Water Vapour for CO2 Adsorption from Flue Gases. *Chem. Eng. J.* **2015**, *281*, 669−677.
(38) Witman, M.; Ling, S.; Jawahery, S.; Boyd, P. G.; Haranczyk, M.; Slater, B.; Smit, B. The Influence of Intrinsic Framework Flexibility on Adsorption in Nanoporous Materials. *J. Am. Chem. Soc.* **2017**, *139* (15), 5547−5557.
(39) Han, S. S.; Goddard, W. A. Metal−Organic Frameworks Provide Large Negative Thermal Expansion Behavior. *J. Phys. Chem. C* **2007**, *111* (42), 15185−15191.
(40) Liang, Z.; Marshall, M.; Chaffee, A. L. CO2 Adsorption-Based Separation by Metal Organic Framework (Cu-BTC) versus Zeolite (13X). *Energy Fuels* **2009**, *23* (5), 2785−2789.
(41) Willems, T. F.; Rycroft, C. H.; Kazi, M.; Meza, J. C.; Haranczyk, M. Algorithms and Tools for High-Throughput Geometry-Based Analysis of Crystalline Porous Materials. *Microporous Mesoporous Mater.* **2012**, *149* (1), 134−141.
(42) Zeeshan, M.; Gulbalkan, H. C.; Haslak, Z. P.; Keskin, S.; Uzun, A. Doubling CO2/N2 Separation Performance of CuBTC by Incorporation of 1-n-Ethyl-3-Methylimidazolium Diethyl Phosphate. *Microporous Mesoporous Mater.* **2021**, *316*, 110947.
(43) Vrtovec, N.; Mazaj, M.; Buscarino, G.; Terracina, A.; Agnello, S.; Arčon, I.; Kovač, J.; Zabukovec Logar, N. Structural and CO2 Capture Properties of Ethylenediamine-Modified HKUST-1 Metal−Organic Framework. *Cryst. Growth Des.* **2020**, *20* (8), 5455−5465.

https://doi.org/10.1021/acsomega.2c05345
ACS Omega 2022, 7, 46515−46523